JOURNAL OF GUIDANCE, CONTROL, AND DYNAMICS
Vol. 23, No. 5, September–October 2000

Linear Theory of a Dual-Spin Projectile in Atmospheric Flight

Mark Costello* and Allen Peterson†
Oregon State University, Corvallis, Oregon 97331

The equations of motion for a dual spin projectile in atmospheric flight are developed and subsequently utilized to examine stability characteristics. The analyzed configuration couples forward and aft body rolling motion with a combination hydrodynamic and roller bearing. By the use of a modified projectile linear theory specialized to this configuration, it is shown that the dynamic stability factor S_D and the gyroscopic stability factor S_G are altered compared to a similar rigid projectile. By the definition of an inertia weighted roll rate, the gyroscopic stability factor takes on the same form as the rigid projectile case. Likewise, by the definition of a Magnus moment weighted roll rate, the dynamic stability factor takes on the same form as the rigid projectile case. For dual-spin projectile configurations with a roller bearing connection, the axial force on each projectile section is required to determine the roll dynamics of both components. This implies that new range reduction algorithms must be developed to estimate the axial force on each projectile section. In contrast, a hydrodynamic bearing does not possess this complication because the roll reaction moment is a function of roll rate difference between the forward and aft bodies.

Nomenclature

$\boldsymbol{a}_{A/I}$ = acceleration of the aft body mass center with respect to the inertial frame
$\boldsymbol{a}_{F/I}$ = acceleration of the forward body mass center with respect to the inertial frame
C^F_{DD}, C^A_{DD} = roll moment aerodynamic coefficient due to fin cant for the forward and aft bodies
C^F_{LP}, C^A_{LP} = roll damping moment aerodynamic coefficient for the forward and aft bodies
C^F_{MQ}, C^A_{MQ} = pitch rate damping moment aerodynamic coefficient for the forward and aft bodies
C^F_{NA}, C^A_{NA} = normal force aerodynamic coefficient for the forward and aft bodies
C^F_{NPA}, C^A_{NPA} = Magnus force aerodynamic coefficient for the forward and aft bodies
C^F_{NR}, C^A_{NR} = yaw rate damping moment aerodynamic coefficient for the forward and aft bodies
C^F_{X0}, C^A_{X0} = zero yaw axial force aerodynamic coefficient for the forward and aft bodies
C^F_{X2}, C^A_{X2} = yaw angle squared axial force aerodynamic coefficient for the forward and aft bodies
C^F_{YB1}, C^A_{YB1} = normal force aerodynamic coefficient along $\boldsymbol{j}_n$ axis for the forward and aft bodies
C^F_{Y0}, C^A_{Y0} = trim side force aerodynamic coefficient for the forward and aft bodies
C^F_{ZB1}, C^A_{ZB1} = normal force aerodynamic coefficient along $\boldsymbol{k}_n$ axis for the forward and aft bodies
C^F_{Z0}, C^A_{Z0} = trim vertical force aerodynamic coefficient for the forward and aft bodies
C_{RB} = friction coefficient for roller bearing
C_V = viscous damping coefficient for hydrodynamic bearing
D = projectile characteristic length
$\boldsymbol{F}_A$ = total externally applied force on the aft body
$\boldsymbol{F}_F$ = total externally applied force on the forward body
I = effective inertia matrix
I_A = mass moment of inertia matrix of the aft body with respect to the aft body reference frame
I_F = mass moment of inertia matrix of the forward body with respect to the forward body reference frame
$\boldsymbol{i}_A, \boldsymbol{j}_A, \boldsymbol{k}_A$ = aft body frame unit vectors
$\boldsymbol{i}_F, \boldsymbol{j}_F, \boldsymbol{k}_F$ = forward body frame unit vectors
$\boldsymbol{i}_N, \boldsymbol{j}_N, \boldsymbol{k}_N$ = fixed plane unit vectors
L_A, M_A, N_A = external moment components on the aft body expressed in the fixed plane reference frame
L_F, M_F, N_F = external moment components on the forward body expressed in the fixed plane reference frame
M_V = roll constraint moment
m = total projectile mass
m_A = aft body mass
m_F = forward body mass
p_A = roll axis component of the angular velocity vector of the aft body expressed in the fixed plane reference frame
p_F = roll axis component of the angular velocity vector of the forward body expressed in the fixed plane reference frame
q, r = components of the angular velocity vector of both the forward and aft bodies expressed in the fixed plane reference frame
q_a = dynamic pressure at the projectile mass center
R_{ax}, R_{ay}, R_{az} = fixed plane components of vector from aft body mass center to aft body center of pressure
$Rm_{ax}, Rm_{ay}, Rm_{az}$ = fixed plane components of vector from aft body mass center to aft body Magnus center of pressure
$Rm_{fx}, Rm_{fy}, Rm_{fz}$ = fixed plane components of vector from forward body mass center to forward body Magnus center of pressure
R_{fx}, R_{fy}, R_{fz} = fixed plane components of vector from forward body mass center to forward body center of pressure
$\bar{r}$ = vector from composite center of mass to central bearing
r_{ax}, r_{ay}, r_{az} = fixed plane components of vector from composite center of mass to aft body mass center
r_{fx}, r_{fy}, r_{fz} = fixed plane components of vector from composite center of mass to forward body mass center
T_A = transformation matrix from the fixed plane reference frame to the aft body reference frame
T_F = transformation matrix from the fixed plane reference frame to the forward body reference frame

Received 22 March 1999; revision received 17 February 2000; accepted for publication 23 February 2000.

*Assistant Professor, Department of Mechanical Engineering. Member AIAA.
†Graduate Research Assistant, Department of Mechanical Engineering; currently Research Engineer, Stirling Technologies, Inc., Kennewick, WA 99336.

u, v, w = translation velocity components of the composite center of mass resolved in the fixed plane reference frame
V = magnitude of mass center velocity
X, Y, Z = total external force components on the composite body expressed in the fixed plane reference frame
x, y, z = position vector components of the composite center of mass expressed in the inertial reference frame
α = longitudinal aerodynamic angle of attack
β = lateral aerodynamic angle of attack
θ, ψ = Euler pitch and yaw angles
$\boldsymbol{\rho}_A$ = distance vector from the aft body mass center to the bearing coupling point
$\boldsymbol{\rho}_F$ = distance vector from the forward body mass center to the bearing coupling point
ϕ_A = Euler roll angle of the aft body
ϕ_F = Euler roll angle of the forward body

Introduction

COMPARED to conventional munitions, the design of smart munitions involves more design requirements stemming from the addition of sensors and control mechanisms. The addition of these components necessitates the minimization of the weight and space impact on the overall projectile design so that desired target effects can still be achieved with the weapon. The inherent design conflict between standard projectile design considerations and new requirements imposed by sensors and control mechanisms has led designers to consider more complex geometric configurations. One such configuration is the dual-spin projectile. This projectile configuration comprises forward and aft components. The forward and aft components are connected through a bearing, which allows the forward and aft portions of the projectile to spin at different rates. Figure 1 shows a schematic of this projectile configuration.

Dual-spin spacecraft dynamics have been extensively studied in the literature. For example, Likins[1] studied the motion of a dual-spin spacecraft and conditions for stability were established. Later, Cloutier[2] obtained an analytical criterion for infinitesimal stability. Along these lines, Mingori[3] as well as Fang[4] considered energy dissipation. Hall and Rand[5] considered spinup dynamics, and resonances occurring during despin were studied by Or.[6] In the latter study, the linear equations governing the resonance dynamics were found to depend on nondimensional parameters related to dynamic unbalance, asymmetry, and the time duration for resonance growth. Other work investigating asymmetric mass properties is due to Cochran et al.,[7] as well as Tsuchiya[8] and Yang.[9] Viderman et al.[10] developed a dynamic model of a dual-spin spacecraft with a flexible platform. Stability was investigated using Floquet theory. Stabb and Schlack[11] investigated the pointing accuracy of a dual-spin spacecraft using the Krylov–Bogoliubov–Mitropolsky perturbation method.

For projectile flight in the atmosphere, aerodynamic forces and moments play a dominant role in the dynamic characteristics. These effects have obviously not been considered in the previous dual-spin spacecraft efforts. However, Smith et al.[12] considered the dynamics of a spin-stabilized artillery projectile modified to accommodate controllable canards mounted to the projectile by a bearing aligned with the spin axis. This work focused on the use of actively controlled canards to reduce miss distance. Both the forward and aft bodies were mass balanced and a hydrodynamic bearing coupled forward and aft body rolling motion.

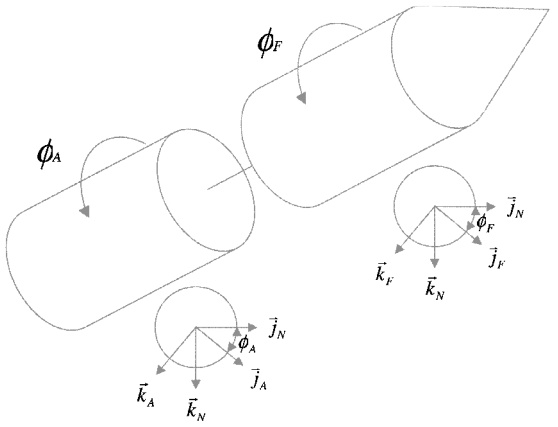

Fig. 1 Dual-spin projectile schematic.

The dual-spin projectile model developed here permits nonsymmetric forward and aft body components and allows a combination of hydrodynamic and roller bearing roll coupling between the forward and aft bodies. By the application of the linear theory for a rigid projectile in atmospheric flight, a dual-spin projectile linear theory is developed. Expressions for the gyroscopic and dynamic stability factors are developed and compared to the rigid projectile case.

Dual-Spin Projectile Dynamic Model

The mathematical model describing the motion of the dual-spin projectile allows for three translational and four rotational rigid-body degrees of freedom. The translational degrees of freedom are the three components of the mass center position vector. The rotational degrees of freedom are the Euler yaw and pitch angles as well as the forward body roll and aft body roll angles. The ground surface is used as an inertial reference frame.[13]

Development of the kinematic and dynamic equations of motion is aided by the use of an intermediate reference frame. The sequence of rotations from the inertial frame to the forward and aft bodies consists of a set of body-fixed rotations that are ordered: yaw, pitch, and forward/aft body roll. The fixed plane reference frame is defined as the intermediate frame before roll rotation. The fixed plane frame is convenient because both the forward and aft bodies share this frame before roll rotation.

Equations (1–4) represent the translational and rotational kinematic and dynamic equations of motion for a dual-spin projectile. Both sets of dynamic equations are expressed in the fixed plane reference frame:

$$\begin{Bmatrix} \dot{x} \\ \dot{y} \\ \dot{z} \end{Bmatrix} = \begin{bmatrix} c_\theta c_\psi & -s_\psi & s_\theta c_\psi \\ c_\theta s_\psi & c_\psi & s_\theta s_\psi \\ -s_\theta & 0 & c_\theta \end{bmatrix} \begin{Bmatrix} u \\ v \\ w \end{Bmatrix} \tag{1}$$

$$\begin{Bmatrix} \dot{\phi}_F \\ \dot{\phi}_A \\ \dot{\theta} \\ \dot{\psi} \end{Bmatrix} = \begin{bmatrix} 1 & 0 & 0 & t_\theta \\ 0 & 1 & 0 & t_\theta \\ 0 & 0 & 1 & 0 \\ 0 & 0 & 0 & 1/c_\theta \end{bmatrix} \begin{Bmatrix} p_F \\ p_A \\ q \\ r \end{Bmatrix} \tag{2}$$

$$\begin{Bmatrix} \dot{u} \\ \dot{v} \\ \dot{w} \end{Bmatrix} = \begin{Bmatrix} X/m \\ Y/m \\ Z/m \end{Bmatrix} - \begin{bmatrix} 0 & -r & q \\ r & 0 & rt_\theta \\ -q & -rt_\theta & 0 \end{bmatrix} \begin{Bmatrix} u \\ v \\ w \end{Bmatrix} \tag{3}$$

$$\begin{Bmatrix} \dot{p}_F \\ \dot{p}_A \\ \dot{q} \\ \dot{r} \end{Bmatrix} = [I]^{-1} \begin{Bmatrix} g_{F1} - M_V \\ g_{A1} + M_V \\ M_2 - S_2^* \\ M_3 - S_3^* \end{Bmatrix} \tag{4}$$

A derivation of Eq. (4) is provided in the Appendix.

Loads on the composite projectile body are due to weight and aerodynamic forces acting on both the forward and aft bodies. Equations (5) and (6) provide expressions for the forward body weight and aerodynamic forces:

$$\begin{Bmatrix} X_W^F \\ Y_W^F \\ Z_W^F \end{Bmatrix} = m_F g \begin{Bmatrix} -s_\theta \\ 0 \\ c_\theta \end{Bmatrix} \tag{5}$$

$$\begin{Bmatrix} X_A^F \\ Y_A^F \\ Z_A^F \end{Bmatrix} = -\tilde{q}_a \begin{Bmatrix} C_{X0}^F + C_{X2}^F \alpha^2 + C_{X2}^F \beta^2 \\ C_{Y0}^F + C_{YB1}^F \beta \\ C_{Z0}^F + C_{ZA1}^F \alpha \end{Bmatrix} \tag{6}$$

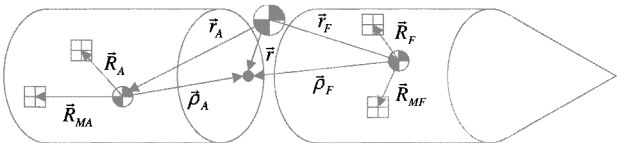

Fig. 2 Dual-spin projectile geometry.

Linear Magnus forces acting on the forward body are formulated separately in Eq. (7). These forces act at the Magnus force center of pressure, which is different from the center of pressure of the steady aerodynamic forces.

$$\begin{Bmatrix} X_M^F \\ Y_M^F \\ Z_M^F \end{Bmatrix} = \tilde{q}_a \begin{Bmatrix} 0 \\ \dfrac{p_F D C_{NPA}^F \alpha}{2V} \\ -\dfrac{p_F D C_{NPA}^F \beta}{2V} \end{Bmatrix} \tag{7}$$

The longitudinal and lateral aerodynamic angles of attack used in Eqs. (6) and (7) are computed using Eqs. (8):

$$\alpha = \tan^{-1}(w/u) \qquad \beta = \tan^{-1}(v/u) \tag{8}$$

$$\tilde{q}_a = \tfrac{1}{8}\rho(u^2 + v^2 + w^2)\pi D^2 \tag{9}$$

Expressions for the aft body forces take on the same form. Aerodynamic coefficients in Eqs. (6) and (7) depend on the local Mach number at the projectile mass center.

The right-hand side of the rotational kinetic equations contains the externally applied moments on both the forward and aft bodies. These equations contain contributions from steady and unsteady aerodynamics. The steady aerodynamic moments are computed for each individual body with a cross product between the steady body aerodynamic force vector and the distance vector from the center of gravity to the center of pressure. Magnus moments on each body are computed in a similar way, with a cross product between the Magnus force vector and the distance vector from the center of gravity to the Magnus center of pressure. Figure 2 shows the relative locations of the forward, aft, and composite body centers of gravity and the forward and aft body centers of pressure. The unsteady body aerodynamic moments provide a damping source for projectile angular motion and are given for the forward body by Eq. (10):

$$\begin{Bmatrix} L_{UA}^F \\ M_{UA}^F \\ N_{UA}^F \end{Bmatrix} = \tilde{q}_a D \begin{Bmatrix} C_{DD}^F + \dfrac{P_F D C_{LP}^F}{2V} \\ \dfrac{q D C_{MQ}^F}{2V} \\ \dfrac{r D C_{NR}^F}{2V} \end{Bmatrix} \tag{10}$$

Air density is computed using the standard atmosphere.[14]

Dual-Spin Projectile Linear Theory

The preceding equations of motion are highly nonlinear and not amenable to a closed-form analytic solution. Linear theory for symmetric rigid projectiles introduces a sequence of assumptions, which yield a tractable set of linear differential equations of motion that can be solved in closed form. These equations form the basis of classic projectile stability theory. The same set of assumptions can be used to establish a linear theory for dual spin projectiles in atmospheric flight:

1) The variables are changed from a fixed plane, station line velocity u, to total velocity V. Equations (11) and (12) relate V and u and their derivatives:

$$V = \sqrt{u^2 + v^2 + w^2} \tag{11}$$

$$\dot{V} = (u\dot{u} + v\dot{v} + w\dot{w})/V \tag{12}$$

2) The variables are changed from time t to dimensionless arclength s. The dimensionless arc length, as defined by Murphy[15] is given in Eq. (13) and has units of calibers of travel:

$$s = \frac{1}{D} \cdot \int_0^t V \cdot \mathrm{d}\tau \tag{13}$$

Equations (14) and (15) relate time and arc length derivatives of a dummy variable ζ. Dotted terms refer to time derivatives and primed terms denote arc length derivatives:

$$\dot{\zeta} = (V/D)\zeta' \tag{14}$$

$$\ddot{\zeta} = (V/D)^2(\zeta'' + \zeta' V'/V) \tag{15}$$

3) Euler yaw and pitch angles are small so that

$$\sin(\theta) \approx \theta \qquad \cos(\theta) \approx 1$$

$$\sin(\psi) \approx \psi \qquad \cos(\psi) \approx 1$$

4) Aerodynamic angles of attack are small so that

$$\alpha \approx w/V \qquad \beta \approx v/V \tag{16}$$

5) The projectile is mass balanced, such that the centers of gravity of both the forward and the aft bodies lie on the rotational axis of symmetry:

$$I_{XY}^A = I_{XY}^F = I_{XZ}^A = I_{XZ}^F = I_{YZ}^A = I_{YZ}^F = 0$$

$$I_{ZZ}^A = I_{YY}^A \qquad I_{ZZ}^F = I_{YY}^F$$

6) The projectile is aerodynamically symmetric such that

$$C_{MQ}^F = C_{NR}^F \qquad C_{MQ}^A = C_{NR}^A$$

$$C_{Y0}^F = C_{Y0}^A = C_{Z0}^F = C_{Z0}^A = 0 \qquad C_{YB1}^F = C_{ZB1}^F = C_{NA}^F$$

$$C_{YB1}^A = C_{ZB1}^A = C_{NA}^A \qquad C_{NA} = C_{NA}^F + C_{NA}^A$$

$$C_{MQ} = C_{MQ}^F + C_{MQ}^A \qquad C_{X0} = C_{X0}^F + C_{X0}^A$$

7) A flat fire trajectory assumption is invoked, and the force of gravity is neglected.

8) The quantities V, ϕ_F, and ϕ_A are large compared to θ, ψ, q, r, v, and w, such that products of small quantities and their derivatives are negligible.

Application of the preceding assumptions results in Eqs. (17–30):

$$x' = D \tag{17}$$

$$y' = (D/V)v + \psi D \tag{18}$$

$$z' = (D/V)w - \theta D \tag{19}$$

$$\phi_F' = (D/V)p_F \tag{20}$$

$$\phi_A' = (D/V)p_A \tag{21}$$

$$\theta' = (D/V)q \tag{22}$$

$$\psi' = (D/V)r \tag{23}$$

$$V' = -[\rho S D/2m](C_{XO})V \tag{24}$$

$$v' = -[\rho S D/2m]\Big\{(C_{NA})v - (D/V)\Big[\Big(C_{NPA}^F/2\Big)p_F + \Big(C_{NPA}^A/2\Big)p_A\Big]w\Big\} - Dr \tag{25}$$

$$w' = -[\rho SD/2m]\Big\{(C_{NA})w + (D/V)\Big[\Big(C^F_{NPA}/2\Big)p_F + \Big(C^A_{NPA}/2\Big)p_A\Big]v\Big\} + Dq \tag{26}$$

$$p'_F = \left[\frac{mD^2}{I^F_{XX}}\right]\left[\frac{\rho SD}{2m}\right]\left\{\left(\frac{V}{D}\right)C^F_{DD} + \frac{C^F_{LP}}{2}p_F - \left(\frac{V}{D}\right)\left[\frac{C_{\mathrm{RB}}\,\mathrm{sign}(p_F - p_A)}{mD}\right]\left|m_F C^A_{X0} - m_A C^F_{X0}\right|\right\} + C_V\left(\frac{D}{V}\right)\frac{(p_A - p_F)}{I^F_{XX}} \tag{27}$$

$$p'_A = \left[\frac{mD^2}{I^A_{XX}}\right]\left[\frac{\rho SD}{2m}\right]\left\{\left(\frac{V}{D}\right)C^A_{DD} + \frac{C^A_{LP}}{2}p_A + \left(\frac{V}{D}\right) \times \left[\frac{C_{\mathrm{RB}}\,\mathrm{sign}(p_F - p_A)}{mD}\right]\left|m_F C^A_{X0} - m_A C^F_{X0}\right|\right\} + C_V\left(\frac{D}{V}\right)\frac{(p_F - p_A)}{I^A_{XX}} \tag{28}$$

$$q' = \left[\frac{\rho SD}{2m}\right]\left[\frac{mD}{I^T_{YY}}\right]\left\{\left(\frac{1}{V}\right)\left[(Rm_{fx} + r_{fx})\frac{C^F_{NPA}}{2}p_F + (Rm_{ax} + r_{ax})\frac{C^A_{NPA}}{2}p_A\right]v + \frac{D}{2}(C_{MQ})q\right\} + \left[\frac{\rho SD}{2m}\right]\left[\frac{mD}{I^T_{YY}}\right]\left\{\left(\frac{1}{D}\right)\left[(R_{fx} + r_{fx})C^F_{NA} + (R_{ax} + r_{ax})C^A_{NA}\right]w\right\} - \frac{D}{V}\frac{\left(I^F_{XX}p_F + I^A_{XX}p_A\right)}{I^T_{YY}}r \tag{29}$$

$$r' = \left[\frac{\rho SD}{2m}\right]\left[\frac{mD}{I^T_{YY}}\right]\left\{\left(\frac{1}{V}\right)\left[(Rm_{fx} + r_{fx})\frac{C^F_{NPA}}{2}p_F + (Rm_{ax} + r_{ax})\frac{C^A_{NPA}}{2}p_A\right]w + \frac{D}{2}(C_{MQ})r\right\} - \left[\frac{\rho SD}{2m}\right]\left[\frac{mD}{I^T_{YY}}\right]\left\{\left(\frac{1}{D}\right)\left[(R_{fx} + r_{fx})C^F_{NA} + (R_{ax} + r_{ax})C^A_{NA}\right]v\right\} + \frac{D}{V}\frac{\left(I^F_{XX}p_F + I^A_{XX}p_A\right)}{I^T_{YY}}q \tag{30}$$

Equations (17–30) are linear, except for the total velocity V, which is retained in several of the equations. Under the assumption that V changes very slowly with respect to the other variables, it is considered to be constant when it appears as a coefficient. With this assumption, the total velocity, the angle of attack dynamics, and the roll dynamics all become uncoupled, linear-time invariant equations of motion. The Magnus force in Eqs. (25) and (26) is typically regarded as small in comparison to the other aerodynamic forces and is shown only for completeness. In further manipulation of the equations, all Magnus forces will be dropped. Magnus moments will be retained, however, due to the magnitude amplification resulting from the cross product between Magnus force and its respective moment arm.

Epicyclic Modes of Oscillation

Equations (17–23) state that the fixed plane is mapped directly onto the inertial reference frame for the given assumptions. Equations (27) and (28) show that a roller bearing model[16,17] requires knowledge of the zero-yaw drag on the forward and aft body separately. Also notice that the Magnus moments appear separately in Eqs. (29) and (30). The equations for total velocity and the fore and aft spin rates have become completely decoupled from the angle-of-attack dynamics. It is a useful result to begin by studying Eq. (24), which represents the total velocity V of the projectile. Equation (24) is separable, and it is elementary to obtain the solution as downrange exponential decay:

$$V(s) = V_0 \exp\{-[(\rho SD/2m)C_{X0}]s\} \tag{31}$$

After we extract the decoupled equations for total velocity and fore and aft spin rates, there are only four equations remaining to examine. These equations describe fixed plane expressions for translational and rotational velocities v, w, q, and r. The angle-of-attack dynamics are driven directly by these four equations because the aerodynamic angles of attack depend on v and w by definition. By the use of Eq. (31) and the definition for small angles of attack given in Eq. (16), the following two relations can be written:

$$\alpha(s) = w(s)/V(s) = [w(s)/V_0]\exp\{[(\rho SD/2m)C_{X0}]s\} \tag{32}$$

$$\beta(s) = v(s)/V(s) = [v(s)/V_0]\exp\{[(\rho SD/2m)C_{X0}]s\} \tag{33}$$

The translational and rotation velocities are described in a compact form as shown in Eq. (34),

$$\begin{Bmatrix} v' \\ w' \\ q' \\ r' \end{Bmatrix} = \begin{bmatrix} -A & 0 & 0 & -D \\ 0 & -A & D & 0 \\ B/D & C/D & E & -F \\ -C/D & B/D & F & E \end{bmatrix}\begin{Bmatrix} v \\ w \\ q \\ r \end{Bmatrix} \tag{34}$$

where

$$A = [\rho SD/2m](C_{NA}) \tag{35}$$

$$B = \left[\frac{\rho SD}{2m}\right]\left[\frac{mD}{I^T_{YY}}\right]\left(\frac{D}{V}\right)\left[(Rm_{fx} + r_{fx})\frac{C^F_{NPA}}{2}p_F + (Rm_{ax} + r_{ax})\frac{C^A_{NPA}}{2}p_A\right] \tag{36}$$

$$C = [\rho SD/2m]\Big[mD\Big/I^T_{YY}\Big]C_{MA} \tag{37}$$

$$E = [\rho SD/2m]\Big[mD^2\Big/I^T_{YY}\Big]C_{MQ}\Big/2 \tag{38}$$

$$F = (D/V)\Big(I^F_{XX}p_F + I^A_{XX}p_A\Big)\Big/I^T_{YY} \tag{39}$$

$$C_{MA} = \Big[(R_{fx} + r_{fx})C^F_{NA} + (R_{ax} + r_{ax})C^A_{NA}\Big] \tag{40}$$

$$I^T_{YY} = I^F_{YY} + m_f r^2_{fx} + I^A_{YY} + m_a r^2_{ax} \tag{41}$$

Eigenvalues of Eq. (34) provide the fast and slow epicyclic modes of oscillation for v, w, q, and r. The four roots of the characteristic equation are displayed hereafter:

$$s = \begin{Bmatrix} \frac{1}{2}\cdot\left[(E - A) + iF \pm \sqrt{(E - A)^2 - F^2 + 4(AE + C) + 2iF\left(E - A + \frac{2(AF + B)}{F}\right)}\right] \\ \frac{1}{2}\cdot\left[(E - A) - iF \pm \sqrt{(E - A)^2 - F^2 + 4(AE + C) - 2iF\left(E - A + \frac{2(AF + B)}{F}\right)}\right] \end{Bmatrix} = \begin{Bmatrix} \lambda_F + i\Phi_F \\ \lambda_S + i\Phi_S \\ \lambda_F - i\Phi_F \\ \lambda_S - i\Phi_S \end{Bmatrix} \tag{42}$$

Linear combinations of the preceding equations lead to Eq. (43):

$$\begin{bmatrix} (E-A) \\ iF \\ -AE-C \\ -i(AF+B) \end{bmatrix} = \begin{bmatrix} \lambda_F + \lambda_S \\ i(\Phi_F + \Phi_S) \\ \lambda_F\lambda_S - \Phi_F\Phi_S \\ i(\lambda_F\Phi_S + \lambda_S\Phi_F) \end{bmatrix} \tag{43}$$

In line with the rigid-body, six-degree-of-freedomprojectile stability analysis, two additional simplifications based on size are introduced. First, neglect the product of the damping factors compared to the product of the damped natural frequencies. Second, neglect the product of A and E because multiples of the relative density factor are small compared with the magnitudes of other terms. A solution may now be obtained for both the fast and the slow damping factors and turning rates for the translational and rotational velocities:

$$\lambda_F = \frac{-(A-E)}{2}\left\{1 + \frac{F}{\sqrt{F^2-4C}}\left[1 - \frac{(2AF+2B)}{F(A-E)}\right]\right\} \tag{44}$$

$$\Phi_F = \frac{1}{2}\left[F + \sqrt{F^2-4C}\right] \tag{45}$$

$$\lambda_S = \frac{-(A-E)}{2}\left\{1 - \frac{F}{\sqrt{F^2-4C}}\left[1 - \frac{(2AF+2B)}{F(A-E)}\right]\right\} \tag{46}$$

$$\Phi_S = \frac{1}{2}\left[F - \sqrt{F^2-4C}\right] \tag{47}$$

Before we draw conclusions about the stability of the angle-of-attack dynamics, the damping factors and the damped natural frequencies have to be calculated for α and β rather than v and w. These new damping factors will account for v, w, and V all decaying downrange. Whether α and β are stable depends on which quantities decay fastest.

Two new damping factors are introduced based on Eqs. (32) and (33):

$$\lambda_F^* = \frac{-[A - 2(\rho SD/2m)C_{X0} - E]}{2}\left(1 + \frac{F}{\sqrt{F^2-4C}} \times \left\{1 - \frac{[2AF + 2(\rho SD/2m)C_{X0}F + 2B]}{F[A - 2(\rho SD/2m)C_{X0} - E]}\right\}\right) \tag{48}$$

$$\lambda_S^* = \frac{-[A - 2(\rho SD/2m)C_{X0} - E]}{2}\left(1 - \frac{F}{\sqrt{F^2-4C}} \times \left\{1 - \frac{[2AF + 2(\rho SD/2m)C_{X0}F + 2B]}{F[A - 2(\rho SD/2m)C_{X0} - E]}\right\}\right) \tag{49}$$

The fast and slow turning rates represent the imaginary parts of the complex eigenvalues. These will remain unchanged for α and β because division by $V(s)$ in Eqs. (32) and (33) only effects the real parts of the eigenvalues. If either ϕ_F or ϕ_S is complex, there will be a positive real part in one of the four eigenvalues. To avoid complex turning rates, the term under the radical in Eqs. (45) and (47) must be greater than zero, which introduces the idea of the gyroscopic stability factor S_G:

$$S_G \equiv (F^2/4 \cdot C) > 1 \tag{50}$$

Furthermore, the dynamic stability factor is defined by Eq. (50):

$$S_D = \frac{[2AF + 2(\rho SD/2m)C_{X0}F + 2B]}{F[A - 2(\rho SD/2m)C_{X0} - E]} \tag{51}$$

The fast mode damping factor λ_F^* must be negative for stable flight. To ensure stability, the following two conditions must be satisfied:

$$[A - 2(\rho SD/2m)C_{X0} - E] > 0 \tag{52}$$

$$1/S_G < S_D(2 - S_D) \tag{53}$$

The results shown in Eqs. (50–53) are very similar to conventional rigid-body projectile analysis. Hence, dual-spin projectile stability analysis can be approached in essentially the same manner that rigid projectiles are analyzed. Differences in stability characteristics arise from the coefficients F and B. The coefficient F contains terms with forward and aft body roll rate and roll inertia appearing separately. Magnus moments also appear separated in the coefficient B, due to their dependence on the forward and aft roll rates.

Dual-Spin Projectile Stability

The gyroscopic and dynamic stability factors can be reexpressed as shown in Eqs. (54) and (55):

$$S_G = \frac{\left(I_{XX}^T \tilde{p}\right)^2}{2I_{YY}^T M} \tag{54}$$

$$S_D = \frac{2(C_{NA} - C_{X0}) + G^T p^*}{(C_{NA} - 2C_{X0}) - \left[mD^2/I_{YY}^T\right](C_{MQ})/2} \tag{55}$$

where

$$\tilde{p} = \frac{(p_F + \gamma_{DS}p_A)}{(1 + \gamma_{DS})} \tag{56}$$

$$\gamma_{DS} = I_{XX}^A / I_{XX}^F \tag{57}$$

$$I_{XX}^T = \left(I_{XX}^F + I_{XX}^A\right) = I_{XX}^F(1 + \gamma_{DS}) \tag{58}$$

$$M = \rho SV^2 C_{MA} \tag{59}$$

$$p^* = \frac{(p_F + \mu_{DS}p_A)}{(1 + \mu_{DS})} \tag{60}$$

$$\mu_{DS} = \frac{(Rm_{ax} + r_{ax})C_{NPA}^A}{(Rm_{fx} + r_{fx})C_{NPA}^F} \tag{61}$$

$$G^T = \left(mD/I_{yy}^T\right)(D/V)\left[(Rm_{fx} + r_{fx})C_{NPA}^F\right](1 + \mu_{DS}) \tag{62}$$

The inertia weighted average spin rate for the composite body $\tilde{p}$ is biased to the spin rate of the body with the largest roll inertia component. The Magnus weighted average spin rate p^* behaves in precisely the same manner as $\tilde{p}$; however, it is biased toward the body with the largest Magnus moment. A plot of $\tilde{p}$ vs roll inertia ratio γ_{DS} and p^* vs Magnus ratio μ_{DS} is shown in Fig. 3. When $\gamma_{DS} = 0$, $\tilde{p}$ is equal to p_F, whereas as $\gamma_{DS} \to \infty$, $\tilde{p}$ approaches p_A. Similar relations hold between μ_{DS} and p^*. Gyroscopic stability factor vs inertia weighted average spin rate is plotted in Fig. 4 for various values of composite inertia and external moments.

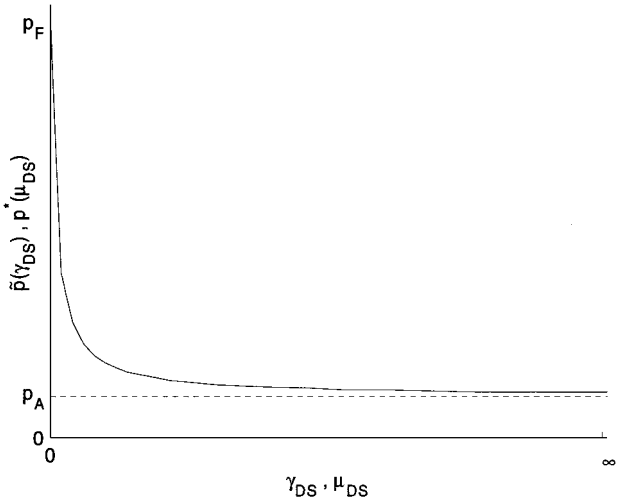

Fig. 3 Inertia weighted average spin rate vs roll inertia ratio.

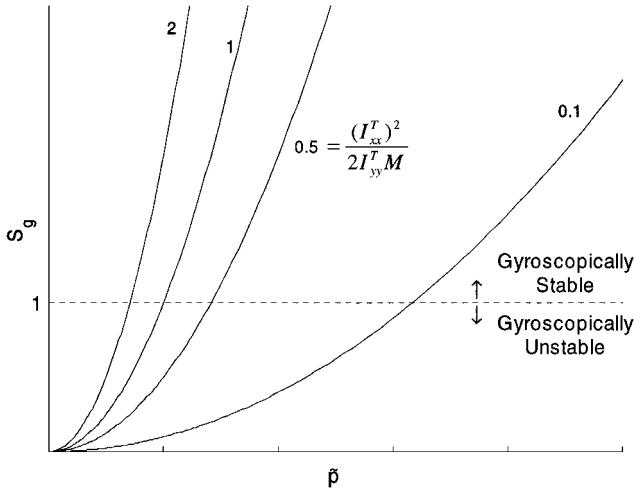

Fig. 4 Gyroscopic stability factor S_G vs inertia weighted average spin rate.

It is interesting to expand Eq. (55) and examine the results. The dynamic stability factor can be broken into two parts. The first part, shown in Eq. (64), represents a stability factor offset that is independent of whether the system is a rigid or dual-spin projectile. Equation (65) shows the second part, which does vary with respect to the rigid-projectile case depending on the Magnus moment coefficients and spin rates. This portion of the total stability factor is directly proportional to the total Magnus moment acting about the composite center of mass and can be considered as a dynamic stability enhancement factor:

$$S_D = H + \Delta_{DS} \tag{63}$$

where

$$H = \left(\frac{2(C_{NA} - C_{X0})}{(C_{NA} - 2C_{X0}) - \left[mD^2 \middle/ I_{YY}^T\right](C_{MQ})/2} \right) \tag{64}$$

$$\Delta_{DS} = \left(\frac{G^T p^*}{(C_{NA} - 2C_{X0}) - \left[mD^2 \middle/ I_{YY}^T\right](C_{MQ})/2} \right) \tag{65}$$

It is also informative to compare the dual-spin projectile stability factors to the conventional rigid-projectile results. To do this, define $\bar{p}$ and Δp as the average spin rate and the spin rate difference, respectively. Thus,

$$p_F = \bar{p} + \Delta p \qquad p_A = \bar{p} - \Delta p$$

The spin rate of an equivalent rigid projectile is $\bar{p}$. The ratio of the dual-spin gyroscopic stability factor to the rigid-projectile gyroscopic stability factor is shown as Eq. (66). Equation (67) shows the ratio of dynamic stability enhancement factors between the dual-spin case and the rigid-projectile case. These two relations are again of very similar form:

$$S_{G_{DS}} \big/ S_G = (1 + [(1 - \gamma_{DS})/(1 + \gamma_{DS})](\Delta p/\bar{p}))^2 \tag{66}$$

$$\Delta_{DS}/\Delta = (1 + [(1 - \mu_{DS})/(1 + \mu_{DS})](\Delta p/\bar{p})) \tag{67}$$

Figures 5 and 6 represent Eq. (66) as a function of the roll inertia ratio and the differential spin ratio. When the gyroscopic stability factor ratio is greater than one, dual-spin gyroscopic stability is enhanced compared to the rigid projectile with a roll rate of $\bar{p}$. It can be shown that the differential spin ratio is positive when the forward body is spinning faster than the aft and negative when the reverse is true. The curves can also be grouped by the roll inertia ratio. When γ_{DS} is less than one, the forward body has more roll inertia. The aft inertia is larger when γ_{DS} is greater than one. Based on the values of the differential spin ratio and roll inertia ratio, Figs. 5 and 6 can viewed in separate quadrants. When both ratios favor one of the bodies, gyroscopic stability is enhanced. When the ratios favor opposite bodies, the stability factor is diminished. Note that the gyroscopic stability ratio can never become negative because the values compared are squared. Also note that in physical systems, the differential spin ratio must be zero when γ_{DS} goes to zero or infinity.

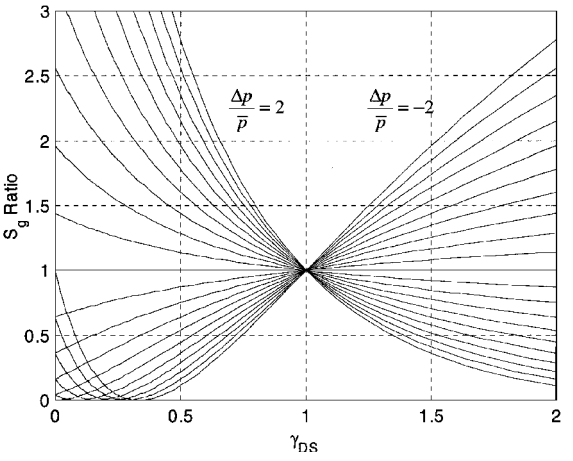

Fig. 5 Gyroscopic stability factor ratio vs γ_{DS}.

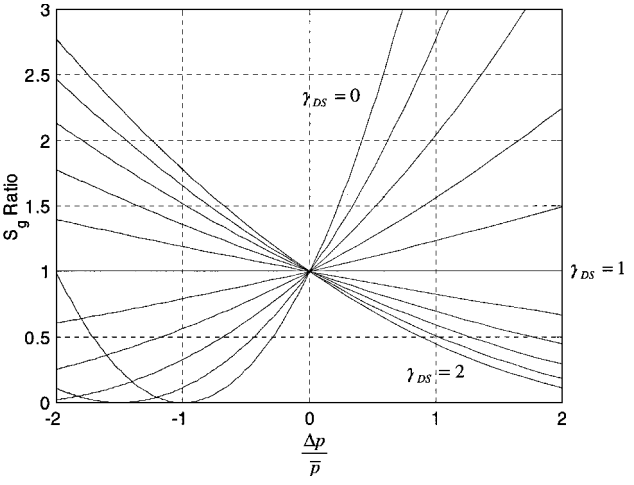

Fig. 6 Gyroscopic stability factor ratio vs differential spin ratio.

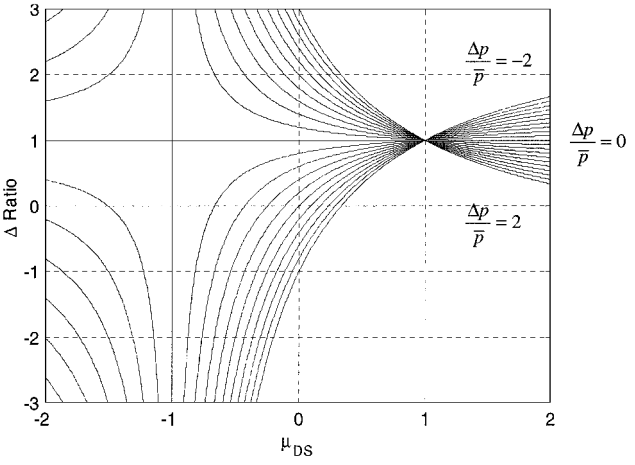

Fig. 7 Delta ratio vs Magnus ratio.

Figures 7 and 8 represent Eq. (66) as a function of the Magnus ratio and the differential spin ratio. When the magnitude of the dynamic enhancement ratio is greater than one, both the total Magnus moment and the dynamic stability enhancement factor are larger than the rigid-projectile case. This can result from several physical situations, which are represented by again considering the graphs in sections.

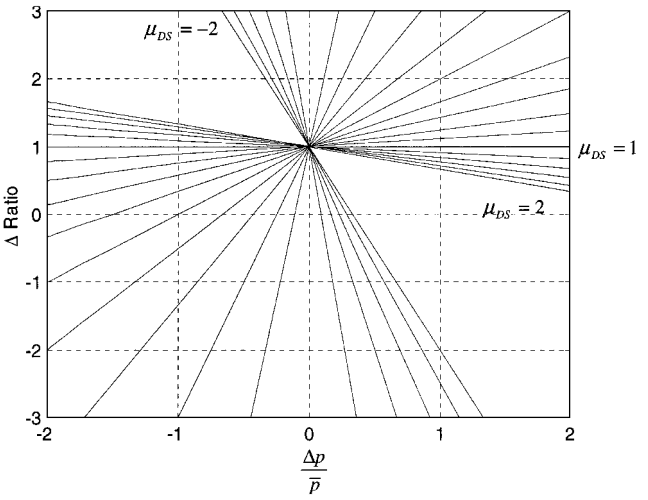

Fig. 8 Delta ratio vs differential spin ratio.

When the Magnus ratio is between negative and positive one, the Magnus moment coefficient is larger for the forward body than for the aft. When the Magnus ratio is outside of these boundaries, the aft body has a larger Magnus coefficient. Negative Magnus ratios indicate that the aft Magnus center of pressure is rearward of the composite body mass center. Positive values of the differential spin ratio again indicate that the forward body is spinning faster than the aft. With this in mind, Figs. 7 and 8 can be viewed where both ratios favor one body, or where they favor opposite bodies. For the first case, the total Magnus moment applied to the dual-spin projectile is larger than that of the rigid case. The opposite is true for the when the ratios favor opposite bodies.

Some special values of Magnus ratio must also be considered. A Magnus ratio equal to one indicates the Magnus coefficients are equivalent or physically that the centers of pressure and force coefficients are equivalent. In this situation, the dual-spin case will have the same Magnus moment as the rigid case because p^* and $\bar{p}$ do not differ. When Magnus ratio is equal to negative one, the Magnus coefficients are equal and opposite. For the rigid case where the bodies spin together, the Magnus moment will go to zero and drive the enhancement ratio to infinity.

Dual-spin projectile stability results must match the standard rigid-projectile stability results in two situations. Either of the bodies may be neglected by setting their mass and inertia properties and force coefficients to zero. In this case, the inertia properties of the total body reduce to those of the remaining body and the roll inertia ratio becomes either 0 or ∞ depending on which body remains. By the use of the same logic, $\bar{p}$ becomes either p_F or p_A. Also, the moments considered, including Magnus, are only those applied to the remaining body. With these assumptions, the rigid body stability results are obtained.

The second case to consider is when the forward and aft bodies spin together. For this case, both the inertia weighted average spin rate and the Magnus weighted average spin rate are equal to both the front and rear spin rates because the projectile bodies are spinning together. This result is true regardless of the roll inertia ratio. The inertia properties are for the total body, as are the applied moments. Again, the rigid-body stability results are obtained.

Conclusions

The equations of motion for a dual-spin projectile in atmospheric flight have been developed. The model allows for unbalanced forward and aft components. The bearing that connects the forward and aft components is a combination hydrodynamic and roller bearing.

After appropriate simplifications are made to the initial nonlinear equations, it is shown that the roller bearing requires knowledge of the axial force on each projectile body in the determination of the roll dynamics. This will require range reduction algorithms to be modified to estimate the axial force on both components from roll angle and roll data. The hydrodynamic bearing does not have this complication because the reaction moment on a hydrodynamic bearing is a function of the roll rate difference only.

It is possible to analyze the stability of a dual-spin projectile using a methodology similar to rigid-body projectile stability analysis. However, the gyroscopic stability factor S_G must be modified compared to the stability factor for a rigid projectile. It depends on the spin rates of both bodies as well as their individual roll inertias. By defining the inertia weighted average spin rate for a dual-spin projectile, the same form of the gyroscopic stability factor for a rigid projectile is obtained. When either the fore or aft body is removed, or both bodies spin together, the stability results reduce to the standard rigid-projectile stability results. The dynamic stability factor S_D is also different from conventional rigid-projectile results. It depends on a Magnus weighted average spin rate. The dynamic stability enhancement ratio depends on the differential spin ratio and the Magnus moment coefficient ratio.

Appendix: Rotation Dynamic Equations

The rotation kinetic differential equations are derived by splitting the two-body system at the bearing connection point. A constraint force $\boldsymbol{F}_C$ and a constraint moment $\boldsymbol{M}_C$ couple the forward and aft bodies. The translational dynamic equations for both bodies are given by Eqs. (A1) and (A2):

$$m_A \boldsymbol{a}_{A/I} = \boldsymbol{F}_A + \boldsymbol{F}_C \tag{A1}$$

$$m_F \boldsymbol{a}_{F/I} = \boldsymbol{F}_F - \boldsymbol{F}_C \tag{A2}$$

Key to the development of the rotation kinetic differential equations is the ability to solve for the constraint forces and moments as a function of state variables and time derivatives of state variables. An expression for the constraint force can be obtained by subtracting Eq. (A2) from Eq. (A1):

$$(m/m_F m_A)\boldsymbol{F}_C = \boldsymbol{F}_F/m_F - \boldsymbol{F}_A/m_A + \boldsymbol{a}_{A/I} - \boldsymbol{a}_{F/I} \tag{A3}$$

With the constraint force known, the rotational dynamic equations for the forward and aft bodies can be developed. The constraint force contributes to the applied moments from a cross product between the constraint force vector and the position vectors from the individual centers of gravity to the bearing. An additional constraint moment couples the forward and aft bodies due to viscous or rolling friction in the bearing:

$$\frac{\mathrm{d}}{\mathrm{d}t}\boldsymbol{H}_{A/I} = \boldsymbol{M}_A + \boldsymbol{M}_V + \boldsymbol{\rho}_A \times \boldsymbol{F}_C \tag{A4}$$

$$\frac{\mathrm{d}}{\mathrm{d}t}\boldsymbol{H}_{F/I} = \boldsymbol{M}_F - \boldsymbol{M}_V + \boldsymbol{\rho}_F \times \boldsymbol{F}_C \tag{A5}$$

where

$$\boldsymbol{\rho}_A = \boldsymbol{r}_A - \bar{r} \tag{A6}$$

$$\boldsymbol{\rho}_F = \boldsymbol{r}_F - \bar{r} \tag{A7}$$

The acceleration of the mass center of the forward and aft bodies, $\boldsymbol{a}_{F/I}$ and $\boldsymbol{a}_{A/I}$, can be expressed in terms of the acceleration of the composite body mass center. After we make this substitution, the constraint force components in the fixed plane reference frame can be expressed in the following manner:

$$\begin{Bmatrix} F_{CX} \\ F_{CY} \\ F_{CZ} \end{Bmatrix} = [F_F] \begin{Bmatrix} \dot{p}_F \\ \dot{q} \\ \dot{r} \end{Bmatrix} + [F_A] \begin{Bmatrix} \dot{p}_A \\ \dot{q} \\ \dot{r} \end{Bmatrix} + \{F_0\} \tag{A8}$$

The constraint moment components in the fixed plane reference frame acting on the forward body about the forward body mass center and resulting from the constraint force cross product can be written in the following manner:

$$\begin{Bmatrix} M_{FC_{FX}} \\ M_{FC_{FY}} \\ M_{FC_{FZ}} \end{Bmatrix} = [M_{FF}] \begin{Bmatrix} \dot{p}_F \\ \dot{q} \\ \dot{r} \end{Bmatrix} + [M_{FA}] \begin{Bmatrix} \dot{p}_A \\ \dot{q} \\ \dot{r} \end{Bmatrix} + \{M_{F0}\} \tag{A9}$$

In a similar way, the components in the fixed plane reference frame of the moment of the constraint force acting on the aft body about the aft body mass center can be written as shown in Eq. (A10):

$$\begin{Bmatrix} M_{FC_{AX}} \\ M_{FC_{AY}} \\ M_{FC_{AZ}} \end{Bmatrix} = [M_{AF}] \begin{Bmatrix} \dot{p}_F \\ \dot{q} \\ \dot{r} \end{Bmatrix} + [M_{AA}] \begin{Bmatrix} \dot{p}_A \\ \dot{q} \\ \dot{r} \end{Bmatrix} + \{M_{A0}\} \quad \text{(A10)}$$

The rotation kinetic differential equations are both expressed in the fixed-plane reference frame. The equations are left general and allow for a fully populated inertia matrix and mass unbalance. Equations (A8–A10) are substituted into both sets of rotation kinetic equations for the forward and aft bodies. At this point, both sets of equations still have unknown constraint moments at the bearing connection point. To eliminate the bearing constraint moments in the fixed plane $\boldsymbol{j}_n$ and $\boldsymbol{k}_n$ directions, the $\boldsymbol{j}_n$ and $\boldsymbol{k}_n$ components of the rotation kinetic equations for the forward and aft bodies are added together to form two dynamic equations that are free of constraint moments. In this way, the constraint moments at the bearing have been eliminated analytically from the pitching and yaw dynamics.

To finish expressing the roll dynamic equations, however, an expression for the unknown constraint moment must be formed. The moment transmitted across the bearing is modeled as a combination hydrodynamic and roller bearing. The contribution from the hydrodynamic bearing can be modeled as viscous damping,[16] and the constitutive relation governing the constraint moment is given by Eq. (A11):

$$M_V^H = c_V(p_F - p_A) \quad \text{(A11)}$$

The frictional moment at a roller bearing is proportional to the normal force acting on the bearing. Normal force at the bearing of a split-bodied projectile is directly related the axial aerodynamic coefficients of the forward and aft bodies. The contribution to the constraint moment from a roller bearing[17] is given by Eq. (A12). To remove the effects of either bearing from the model, set the respective coefficient to zero:

$$M_V^R = C_{\mathrm{RB}}|F_{CX}|\,\mathrm{sign}(p_F - p_A) \quad \text{(A12)}$$

Once the final constraint moment is known, the fixed plane $\boldsymbol{i}_n$ components of Eqs. (A4) and (A5) are the forward and aft body roll dynamic equations. These two individual equations, in conjunction with the fixed plane $\boldsymbol{j}_n$ and $\boldsymbol{k}_n$ equations, which result from a sum of Eqs. (A4) and (A5), can be assembled to represent the entire set of rotational dynamics. Equation (4) is restated to demonstrate this point:

$$\begin{bmatrix} I_{1,1} & I_{1,2} & I_{1,3} & I_{1,4} \\ I_{2,1} & I_{2,2} & I_{2,3} & I_{2,4} \\ I_{3,1} & I_{3,2} & I_{3,3} & I_{3,4} \\ I_{4,1} & I_{4,2} & I_{4,3} & I_{4,4} \end{bmatrix} \begin{Bmatrix} \dot{p}_F \\ \dot{p}_A \\ \dot{q} \\ \dot{r} \end{Bmatrix} = \begin{Bmatrix} g_{F1} - M_V \\ g_{A1} + M_V \\ M_2 - S_2^* \\ M_3 - S_3^* \end{Bmatrix}$$

The effective inertia matrix is a 4×4 matrix that is a combination of the inertia matrices of both the forward and aft bodies. As an aid in developing a formula for the effective inertia matrix, define the following intermediate matrices:

$$I_A^* = \bar{I}_A - \tilde{I}_A \quad \text{(A13)}$$

$$\bar{I}_A = T_A^T I_A T_A \quad \text{(A14)}$$

$$\tilde{I}_A = m_A S_{RA} S_{RA} \quad \text{(A15)}$$

$$I_F^* = \bar{I}_F - \tilde{I}_F \quad \text{(A16)}$$

$$\bar{I}_F = T_F^T I_F T_F \quad \text{(A17)}$$

$$\tilde{I}_F = m_F S_{RF} S_{RF} \quad \text{(A18)}$$

where

$$T_F = \begin{bmatrix} 1 & 0 & 0 \\ 0 & c_{\phi_F} & s_{\phi_F} \\ 0 & -s_{\phi_F} & s_{\phi_F} \end{bmatrix} \quad \text{(A19)}$$

$$T_A = \begin{bmatrix} 1 & 0 & 0 \\ 0 & c_{\phi_A} & s_{\phi_A} \\ 0 & -s_{\phi_A} & s_{\phi_A} \end{bmatrix} \quad \text{(A20)}$$

$$S_{RF} = \begin{bmatrix} 0 & -r_{fz} & r_{fy} \\ r_{fz} & 0 & -r_{fx} \\ -r_{fy} & r_{fx} & 0 \end{bmatrix} \quad \text{(A21)}$$

$$S_{RA} = \begin{bmatrix} 0 & -r_{az} & r_{ay} \\ r_{az} & 0 & -r_{ax} \\ -r_{ay} & r_{ax} & 0 \end{bmatrix} \quad \text{(A22)}$$

By the use of Eqs. (A13), (A16), (A11), and (A12), elements of the effective inertia matrix can now be formed:

$$I_{1,1} = I_{F_{1,1}}^* + M_{FF_{1,1}} \quad \text{(A23)}$$

$$I_{1,2} = M_{FA_{1,1}} \quad \text{(A24)}$$

$$I_{1,3} = I_{F_{1,2}}^* + M_{FF_{1,2}} + M_{FA_{1,2}} \quad \text{(A25)}$$

$$I_{1,4} = I_{F_{1,3}}^* + M_{FF_{1,3}} + M_{FA_{1,3}} \quad \text{(A26)}$$

$$I_{2,1} = M_{AF_{1,1}} \quad \text{(A27)}$$

$$I_{2,2} = I_{A_{1,1}}^* - M_{AA_{1,1}} \quad \text{(A28)}$$

$$I_{2,3} = I_{A_{1,2}}^* - M_{AA_{1,2}} - M_{AF_{1,2}} \quad \text{(A29)}$$

$$I_{2,4} = I_{A_{1,3}}^* - M_{AA_{1,3}} - M_{AF_{1,3}} \quad \text{(A30)}$$

$$I_{3,1} = I_{F_{2,1}}^* \quad \text{(A31)}$$

$$I_{3,2} = I_{A_{2,1}}^* \quad \text{(A32)}$$

$$I_{3,3} = I_{F_{2,2}}^* + I_{A_{2,2}}^* \quad \text{(A33)}$$

$$I_{3,4} = I_{F_{2,3}}^* + I_{A_{2,3}}^* \quad \text{(A34)}$$

$$I_{4,1} = I_{F_{3,1}}^* \quad \text{(A35)}$$

$$I_{4,2} = I_{A_{3,1}}^* \quad \text{(A36)}$$

$$I_{4,3} = I_{F_{3,2}}^* + I_{A_{3,2}}^* \quad \text{(A37)}$$

$$I_{4,4} = I_{F_{3,3}}^* + I_{A_{3,3}}^* \quad \text{(A38)}$$

Two scalar elements of the right-hand-side vector of Eq. (4) are given by Eqs. (A39) and (A40):

$$g_{F_1} = [1 \quad 0 \quad 0]\left[M_F - S_F^* - M_{F0}\right] \quad \text{(A39)}$$

$$g_{A_1} = [1 \quad 0 \quad 0]\left[M_A - S_A^* - M_{A0}\right] \quad \text{(A40)}$$

The vectors $\boldsymbol{S}_A^*$ and $\boldsymbol{S}_F^*$ in Eqs. (A39) and (A40) are given by Eqs. (A41) and (A44):

$$\boldsymbol{S}_A^* = \bar{S}_A - \tilde{S}_A \quad \text{(A41)}$$

$$\bar{S}_A = \left[T_A^T I_A \dot{T}_A + T_A^T S_A I_A T_A\right] \begin{Bmatrix} p_a \\ q \\ r \end{Bmatrix} \quad \text{(A42)}$$

$$\tilde{S}_A = \left[\tilde{I}_A T_A^T \dot{T}_A + m_A S_{RA} S_A S_{RA}\right] \begin{Bmatrix} p_a \\ q \\ r \end{Bmatrix} \quad \text{(A43)}$$

$$S_F^* = \bar{S}_F - \tilde{S}_F \quad \text{(A44)}$$

$$\bar{S}_F = \left[T_F^T I_F \dot{T}_F + T_F^T S_F I_F T_F\right] \begin{Bmatrix} p_f \\ q \\ r \end{Bmatrix} \quad \text{(A45)}$$

$$\tilde{S}_F = \left[\tilde{I}_F T_F^T \dot{T}_F + m_F S_{RF} S_F S_{RF}\right] \begin{Bmatrix} p_f \\ q \\ r \end{Bmatrix} \tag{A46}$$

where

$$S_F = \begin{bmatrix} 0 & s_{\phi_F} q - c_{\phi_F} r & c_{\phi_F} q + s_{\phi_F} r \\ c_{\phi_F} r - s_{\phi_F} q & 0 & -p_F \\ -c_{\phi_F} q - s_{\phi_F} r & p_F & 0 \end{bmatrix}$$

$$S_A = \begin{bmatrix} 0 & s_{\phi_A} q - c_{\phi_A} r & c_{\phi_A} q + s_{\phi_A} r \\ c_{\phi_A} r - s_{\phi_A} q & 0 & -p_A \\ -c_{\phi_A} q - s_{\phi_A} r & p_A & 0 \end{bmatrix}$$

$$\dot{T}_F = \begin{bmatrix} 0 & 0 & 0 \\ 0 & -(p_F + t_\theta r) s_{\phi_F} & (p_F + t_\theta r) c_{\phi_F} \\ 0 & -(p_F + t_\theta r) c_{\phi_F} & -(p_F + t_\theta r) s_{\phi_F} \end{bmatrix}$$

$$\dot{T}_A = \begin{bmatrix} 0 & 0 & 0 \\ 0 & -(p_A + t_\theta r) s_{\phi_A} & (p_A + t_\theta r) c_{\phi_A} \\ 0 & -(p_A + t_\theta r) c_{\phi_A} & -(p_A + t_\theta r) s_{\phi_A} \end{bmatrix}$$

Other unknown terms on the right-hand side of Eq. (4) include components of the vectors $\boldsymbol{M}$ and $\boldsymbol{S}^*$. These vectors are described here:

$$S^* = S_F^* + S_A^* = \begin{Bmatrix} S_1^* \\ S_2^* \\ S_3^* \end{Bmatrix} \tag{A47}$$

$$M = M_F + M_A = \begin{Bmatrix} M_1 \\ M_2 \\ M_3 \end{Bmatrix} \tag{A48}$$

References

[1]Likins, P. W., "Attitude Stability Criteria for Dual-Spin Spacecraft," *Journal of Spacecraft and Rockets*, Vol. 4, No. 12, 1967, pp. 1638–1643.

[2]Cloutier, G. J., "Stable Rotation States of Dual-Spin Spacecraft," *Journal of Spacecraft and Rockets*, Vol. 5, No. 4, 1968, pp. 490–492.

[3]Mingori, D. L., "Effects of Energy Dissipation on the Attitude Stability of Dual-Spin Satellites," *AIAA Journal*, Vol. 7, No. 10, 1969, pp. 20–27.

[4]Fang, B. T., "Energy Considerations for Attitude Stability of Dual-Spin Spacecraft," *Journal of Spacecraft and Rockets*, Vol. 5, No. 5, 1968, pp. 1241–1243.

[5]Hall, C. D., and Rand, R. H., "Spinup Dynamics of Axial Dual-Spin Spacecraft," *Journal of Guidance, Control, and Dynamics*, Vol. 17, No. 1, 1994, pp. 30–37.

[6]Or, A. C., "Resonances in the Despin Dynamics of Dual-Spin Spacecraft," *Journal of Guidance, Control, and Dynamics*, Vol. 14, No. 2, 1991, pp. 321–329.

[7]Cochran, J. E., Shu, P. H., and Rew, S. D., "Attitude Motion of Asymmetric Dual-Spin Spacecraft," *Journal of Guidance, Control, and Dynamics*, Vol. 5, No. 1, 1982, pp. 37–42.

[8]Tsuchiya, K., "Attitude Behavior of a Dual-Spin Spacecraft Composed of Asymmetric Bodies," *Journal of Guidance, Control, and Dynamics*, Vol. 2, No. 4, 1979, pp. 328–333.

[9]Yang, H. X., "Method for Stability Analysis of Asymmetric Dual-Spin Spacecraft," *Journal of Guidance, Control, and Dynamics*, Vol. 12, No. 1, 1989, pp. 123–125.

[10]Viderman, Z., Rimrott, F. P. J., and Cleghorn, W. L., "Stability of an Asymmetric Dual-Spin Spacecraft with Flexible Platform," *Journal of Guidance, Control, and Dynamics*, Vol. 14, No. 4, 1991, pp. 751–760.

[11]Stabb, M. C., and Schlack, A. L., "Pointing Accuracy of a Dual-Spin Satellite due to Torsional Appendage Vibrations," *Journal of Guidance, Control, and Dynamics*, Vol. 16, No. 4, 1991, pp. 630–635.

[12]Smith, J. A., Smith, K. A., and Topliffe, R., "Feasibility Study for Application of Modular Guidance and Control Units to Existing ICM Projectiles," Final Technical Rept., Contractor Rept., ARLCD-CR-79001, U.S. Army Armament Research and Development Command, Picatinny Arsenal, Dover, NJ, 1978.

[13]Etkin, B., *Dynamics of Atmospheric Flight*, Wiley, New York, 1972, Chap. 4.

[14]Von Mises, R., *Theory of Flight*, Dover, New York, 1959, Chap. 1.

[15]Murphy, C. H., "Free Flight Motion of Symmetric Missiles," U.S. Army Research Lab. Rept. 1216, Aberdeen Proving Ground, MD, 1963.

[16]Close, C. M., and Frederick, D. K., *Modeling and Analysis of Dynamic Systems*, Wiley, New York, 1995, Chap. 2.

[17]Bolz, R. E., and Tuve, G. L., *CRC Handbook of Tables for Applied Engineering Science*, CRC Press, Boca Raton, FL, 1973, Sec. 6.2.